Mathematical Biosciences and Engineering

MBE, 19(1): 351–370.
DOI: 10.3934/mbe.2022018
Received: 25 August 2021
Accepted: 17 October 2021
Published: 15 November 2021

http://www.aimspress.com/journal/MBE

Research article

Numerical investigations of the nonlinear smoke model using the Gudermannian neural networks

Zulqurnain Sabir[1], Muhammad Asif Zahoor Raja[2], Abeer S. Alnahdi[3,*], Mdi Begum Jeelani[3] and M. A. Abdelkawy [3,4,*]

[1] Department of Mathematics and Statistics, Hazara University, Mansehra, Pakistan
[2] Future Technology Research Center, National Yunlin University of Science and Technology, 123 University Road, Section 3, Douliou, Yunlin 64002, Taiwan, R.O.C.
[3] Department of Mathematics and Statistics, Faculty of Science, Imam Mohammad Ibn Saud Islamic University, Riyadh, Saudi Arabia
[4] Department of Mathematics, Faculty of Science, Beni-Suef University, Beni-Suef, Egypt

* **Correspondence:** maohamed@imamu.edu.sa, asalnahdi@imamu.edu.sa.

Abstract: These investigations are to find the numerical solutions of the nonlinear smoke model to exploit a stochastic framework called gudermannian neural works (GNNs) along with the optimization procedures of global/local search terminologies based genetic algorithm (GA) and interior-point algorithm (IPA), i.e., GNNs-GA-IPA. The nonlinear smoke system depends upon four groups, temporary smokers, potential smokers, permanent smokers and smokers. In order to solve the model, the design of fitness function is presented based on the differential system and the initial conditions of the nonlinear smoke system. To check the correctness of the GNNs-GA-IPA, the obtained results are compared with the Runge-Kutta method. The plots of the weight vectors, absolute error and comparison of the results are provided for each group of the nonlinear smoke model. Furthermore, statistical performances are provided using the single and multiple trial to authenticate the stability and reliability of the GNNs-GA-IPA for solving the nonlinear smoke system.

Keywords: Gudermannain neural networks; nonlinear smoke model; Runge-Kutta; active-set algorithm; genetic algorithms; numerical results

1. Introduction

According to the reports of the World Health Organization (WHO), there are many deaths occur using the tobacco epidemic and its prey most of the disabled persons during some past few years. The tobacco epidemic not only disturbs the individuals, but also become a reason for increases the health care cost, delays financial development and decreases the families' budgets [1]. The chain smoking is a big reason of death due to oral cavity cancer, bladder, larynx, esophagus, lung, stomach, pancreas, renal pelvis and cervix. The smoking also creates the problems of heart, chronic obstructive, lung weakness, breathing diseases, peripheral vascular and less weight of newly born children. WHO also reports that the reasoning of unproductive pregnancies, peptic ulcer disease and increase the infant mortality rate is due to smoking [2]. The termination of smoking is an instantaneous health support and dramatically reduces the danger of many deathly diseases and improve the respiratory system of the younger. It is the obligation of the higher authorities to teach their people and aware the communities about the drawbacks of smoking as well as develop an active policy to control this habit. Castillo et al. [3] discussed the mathematical model to avoid the smoking by considering the population into two kings, i.e., smokers (S) and those individuals who left smoking permanently (QP). In addition, Shoromi et al. [4] presented a new group temporary smoker (QT) in this mathematical model, which is defined as:

$$\begin{cases} P^{'}(\Omega) = \mu(1 - P(\Omega)) - \beta P(\Omega)S(\Omega), P(0) = l_1, \\ S^{'}(\Omega) = \beta P(\Omega)S(\Omega) - (\gamma + \mu)S(\Omega) + \alpha Q_T(\Omega), S(0) = l_2, \\ Q_T^{'}(\Omega) = \gamma(1 - \sigma)S(\Omega) - (\mu + \alpha)Q_T(\Omega), Q_T(0) = l_3, \\ Q_P^{'}(\Omega) = -\mu Q_P(\Omega) + \gamma\sigma S(\Omega), Q_P(0) = l_4, \end{cases} \tag{1}$$

where $P(\Omega)$, $S(\Omega)$, $Q_T(\Omega)$ and $Q_P(\Omega)$ indicate the Potential smoker (P) group, Smoker (S) group, Temporary smoker (QT) group and Permanent smoker (QS) group at time Ω. Whereas,$\sigma, \alpha, \gamma, \beta$ and μ represent the positive values of the constants. Furthermore, l_1, l_2, l_3 and l_4 designate the initial conditions (ICs) of the nonlinear smoke model (1).

The aim of this work is to investigate the nonlinear smoke model numerically to exploit a stochastic framework called Gudermannian neural works (GNNs) [5–8] along with the optimization procedures of global/local search terminologies based Genetic algorithm (GA) and interior-point approach (IPA), i.e., GNNs-GA-IPA. The development of the numerical solvers has been reported in various proposals for the solution of the linear/nonlinear differential models with their own applicability, stability and significance [9–13], however recently artificial intelligence based numerical computing platform are introduction as a promising alternatives [14–18]. Whereas, GNNs-GA-IPA is never been applied before to solve the nonlinear smoke system. Some recent proposals of the stochastic solvers are functional singular system [19], nonlinear SIR dengue fever model [20], mathematical models of environmental economic systems [21], prey-predator nonlinear system [22], Thomas-Fermi system [23], mosquito dispersal model [24], transmission of heat in human head [25], multi-singular fractional system [26] and nonlinear COVID-19 model [27]. Some novel prominent features of the current investigations are provided as:

- The GNNs are explored efficaciously using the hybrid optimization paradigm based on GA-IPA for solving the nonlinear smoke model.
- The consistent overlapped outcomes obtained by GNNs-GA-IPA and the Runge-Kutta numerical

results validate the correctness and exactness of the proposed scheme.

- The authorization of the performance is accomplished through different statistical valuations to attain the numerical outcomes of the nonlinear smoke system.

The benefits, merits and noteworthy contributions of the GNNs-GA-IPA are simply implemented to solve the nonlinear smoke model, understanding easiness, operated efficiently and inclusive with reliable applications in diversified fields.

The remaining parts of the current work are studied as: Section 2 defines the procedures of GNNs-GA-IPA along with and statistical measures. Section 3 indicates the results simulations. Section 4 provided the final remarks and future research reports.

2. Designed methodology

In this section, the proposed form of the GNNs-GA-IPA is presented in two steps to solve the nonlinear smoke model as:

- A merit function is designed using the differential system and ICs of the nonlinear smoke system.
- The necessary and essential settings are provided for the optimization procedures of GA-IPA to solve the nonlinear smoke model.

2.1. Structure of GNN-GA-IPA

In this section, the mathematical formulations to solve the nonlinear smoke model-based groups, Potential smoker ($\hat{P}$), Temporary smoker ($\hat{Q}_T$), Permanent smoker ($\hat{Q}_S$) and Smoker ($\hat{S}$) are presented. The proposed results of these groups of the nonlinear smoke model, $\hat{P}$, $\widehat{S}$, $\widehat{Q}_T$ and $\widehat{Q}_S$ are represented by $\hat{P}$, $\widehat{S}$, $\widehat{Q}_T$ and $\widehat{Q}_S$ together with their derivatives are written as:

$$[\hat{P}(\Omega),\, \widehat{S}(\Omega),\, \widehat{Q}_T(\Omega),\, \widehat{Q}_S(\Omega)] = \begin{bmatrix} \sum_{i=1}^{m} k_{P,i} T(w_{P,i}\Omega + h_{P,i}),\, \sum_{i=1}^{m} a_{S,i} T(w_{S,i}\Omega + h_{S,i}), \\ \sum_{i=1}^{m} a_{Q_T,i} T(w_{Q_T,i}\Omega + h_{Q_T,i}),\, \sum_{i=1}^{m} a_{Q_S,i} T(w_{Q_S,i}\Omega + h_{Q_S,i}) \end{bmatrix}, \tag{2}$$

$$[\hat{P}'(\Omega),\, \hat{S}'(\Omega),\, \widehat{Q}_T'(\Omega),\, \widehat{Q}_S'(\Omega)] = \begin{bmatrix} \sum_{i=1}^{m} k_{P,i} T'(w_{P,i}\Omega + h_{P,i}),\, \sum_{i=1}^{m} k_{S,i} T'(w_{S,i}\Omega + h_{S,i}), \\ \sum_{i=1}^{m} k_{Q_T,i} T'(w_{Q_T,i}\Omega + h_{Q_T,i}),\, \sum_{i=1}^{m} k_{Q_S,i} T'(w_{Q_S,i}\Omega + h_{Q_S,i}) \end{bmatrix}.$$

where W is the unknown weight vector, written as:

$W = [W_P,\, W_S,\, W_{Q_T},\, W_{Q_S}]$, for $W_P = [k_P,\, \omega_P,\, h_P]$, $W_S = [k_S,\, \omega_S,\, h_S]$, $W_{Q_T} = [k_{Q_T},\, \omega_{Q_T},\, h_{Q_T}]$

and $W_{Q_S} = [k_{Q_S},\, \omega_{Q_S},\, h_{Q_S}]$, where

$k_P = [k_{P,1},\, k_{P,2},\ldots,\, k_{P,m}]$, $k_S = [k_{S,1},\, k_{S,2},\ldots,\, k_{S,m}]$, $k_{Q_T} = [k_{Q_T,1},\, k_{Q_T,2},\ldots,\, k_{Q_T,m}]$, $k_{Q_S} =$

$[k_{Q_S,1},\, k_{Q_T,2},\ldots,\, k_{Q_T,m}]$, $w_P = [w_{P,1},\, w_{P,2},\ldots,\, w_{P,m}]$, $w_S = [w_{S,1},\, w_{S,2},\ldots,\, w_{S,m}]$ $w_{Q_T} =$

$[w_{Q_T,1},\, w_{Q_T,2},\ldots,\, w_{Q_T,m}]$, $w_{Q_S} = [w_{Q_S,1},\, w_{Q_T,2},\ldots,\, w_{Q_T,m}]$, $h_P = [h_{P,1},\, h_{P,2},\ldots,\, h_{P,m}]$ $h_S =$

$[h_{S,1}, h_{S,2},\ldots, h_{S,m}]$, $h_{Q_T} = [h_{Q_T,1}, h_{Q_T,2},\ldots, h_{Q_T,m}]$, $h_{Q_S} = [h_{Q_S,1}, h_{Q_T,2},\ldots, h_{Q_T,m}]$

The Gudermannian function $T(\Omega) = 2\,tan^{-1}[exp(\Omega)] - 0.5\pi$ is applied in the above model, this GNNs have never been implemented before the solve this model.

$$\begin{bmatrix} \hat{P}(\Omega), & \hat{S}(\Omega), \\ \hat{Q}_T(\Omega), & \hat{Q}_S(\Omega) \end{bmatrix} =$$

$$\begin{bmatrix} \sum_{i=1}^{m} k_{P,i}\left(2\,tan^{-1}\,e^{(w_{P,i}\Omega+h_{P,i})} - \frac{\pi}{2}\right), \sum_{i=1}^{m} k_{S,i}\left(2\,tan^{-1}\,e^{(w_{S,i}\Omega+h_{S,i})} - \frac{\pi}{2}\right), \\ \sum_{i=1}^{m} k_{Q_T,i}\left(2\,tan^{-1}\,e^{(w_{Q_T,i}\Omega+h_{Q_T,i})} - \frac{\pi}{2}\right), \sum_{i=1}^{m} k_{Q_P,i}\left(2\,tan^{-1}\,e^{(w_{Q_S,i}\Omega+h_{Q_S,i})} - \frac{\pi}{2}\right) \end{bmatrix},$$

$$\begin{bmatrix} \hat{P}'(\Omega), & \hat{S}'(\Omega), \\ \hat{Q}_T'(\Omega), & \hat{Q}_S'(\Omega) \end{bmatrix} = \tag{3}$$

$$\begin{bmatrix} \sum_{i=1}^{m} 2k_{P,i}w_{P,i}\left(\frac{e^{(w_{p,i}\Omega+n_{p,i})}}{1+\left(e^{(w_{p,i}\Omega+n_{p,i})}\right)^2}\right), \sum_{i=1}^{m} 2k_{S,i}w_{S,i}\left(\frac{e^{(w_{S,i}\Omega+n_{S,i})}}{1+\left(e^{(w_{S,i}\Omega+n_{S,i})}\right)^2}\right), \\ \sum_{i=1}^{m} 2k_{Q_T,i}w_{Q_T,i}\left(\frac{e^{(w_{Q_T,i}\Omega+n_{Q_T,i})}}{1+\left(e^{(w_{Q_T,i}\Omega+n_{Q_T,i})}\right)^2}\right), \sum_{i=1}^{m} 2k_{Q_S,i}w_{Q_S,i}\left(\frac{e^{(w_{Q_S,i}\Omega+n_{Q_S,i})}}{1+\left(e^{(w_{Q_S,i}\Omega+n_{Q_S,i})}\right)^2}\right) \end{bmatrix},$$

For the process of optimization, a fitness function is given as:

$$\Xi_{Fit} = \Xi_1 + \Xi_2 + \Xi_3 + \Xi_4 + \Xi_5, \tag{4}$$

$$\Xi_1 = \frac{1}{N}\sum_{i=1}^{N}\left[\hat{P}_i' - \mu + \mu\hat{P}_i + \beta\hat{P}_i\hat{S}_i\right]^2, \tag{5}$$

$$\Xi_2 = \frac{1}{N}\sum_{i=1}^{N}\left[\hat{S}_i' - \beta\hat{P}_i\hat{S}_i + \mu\hat{S}_i + \gamma\hat{S}_i - \alpha\left(\hat{Q}_T\right)_i\right]^2, \tag{6}$$

$$\Xi_3 = \frac{1}{N}\sum_{i=1}^{N}\left[\left(\hat{Q}_T'\right)_i + \gamma\sigma\hat{S}_i - \gamma\hat{S}_k + \alpha\left(\hat{Q}_T\right)_i + \mu\left(\hat{Q}_T\right)_i\right]^2, \tag{7}$$

$$\Xi_4 = \frac{1}{N}\sum_{i=1}^{N}\left[\left(\hat{Q}_P'\right)_i - \gamma\sigma\hat{S}_i + \mu\left(\hat{Q}_P\right)_i\right]^2, \tag{8}$$

$$\Xi_5 = \frac{1}{4}\left[\left(\hat{P}_0 - l_1\right)^2 + \left(\hat{S}_0 - l_2\right)^2 + \left((\hat{Q}_T)_0 - l_3\right)^2 + +\left((\hat{Q}_S)_0 - l_4\right)^2\right], \tag{9}$$

where $\hat{P}_i = P(\Omega_i)$, $\hat{S}_i = S(\Omega_i)$, $(Q_T)_i = Q_T(\Omega_i)$, $(Q_S)_i = Q_S(\Omega_i)$, $TN = 1$, and $\Omega_i = ih$. The error functions Ξ_1, Ξ_2, Ξ_3 and Ξ_4 are related to system (1), while, Ξ_5 is based on the ICs of the nonlinear smoke model (1).

2.2. Optimization procedures: GA-IPA

In this section, the performance of the scheme is observed using the optimization process of GA-IPA to solve the nonlinear smoke system. The designed GNNs-GA-IPA methodology based on the nonlinear smoke system is illustrated in Figure 1.

Table 1. The procedure of optimization using the GNNs-GA-IPA for the nonlinear smoke model.

GA process starts

Inputs: The chromosomes of the same network elements are denoted as:

W = $[k,\ w,\ h]$

Population: Chromosomes set is represented as:

$W = [W_P,\ W_S,\ W_{Q_T},\ W_{Q_S}], W_P = [k_P,\ \omega_P,\ h_P], W_S = [k_S,\ \omega_S,\ h_S], W_{Q_T} = \left[k_{Q_T},\ \omega_{Q_T},\ h_{Q_T}\right]$

and $W_{Q_S} = [k_{Q_S},\ \omega_{Q_S},\ h_{Q_S}]$, W is the weight vector

Outputs: The best global weight values are signified as: $W_{GA\text{-}Best}$

Initialization: For the chromosome's assortment, adjust the W

Assessment of FIT: Adjust "Ξ_{Fit}" in the population (P) for each vector values using Eqs (4)–(9).

- Stopping standards: Terminate if any of the criteria is achieved [$\Xi_{Fit} = 10^{-19}$], [Generataions = 120] [TolCon = TolFun = 10^{-18}], [StallLimit = 150], & [Size of population = 270].

Move to [storage]

Ranking: Rank precise W in the particular population for Ξ_{Fit}.

Storage: Save Ξ_{Fit}, iterations, $W_{GA\text{-}Best}$, function counts and time.

GA procedure End

Start of IPA

Inputs: $W_{GA\text{-}Best}$ is selected as an initial point.

Output: $W_{GA\text{-}IPA}$ shows the best weights of GA-IPA.

Initialize: $W_{GA\text{-}Best}$, generations, assignments and other standards.

Terminating criteria: Stop if [Ξ_{Fit} = 10-20], [TolFun = 10-18], [Iterations = 700], [TolCon = TolX = 10-22] and [MaxFunEvals = 260000] attained.

Evaluation of Fit: Compute the values of W and E for Eqs (4)–(9).

Amendments: Normalize 'fmincon' for IPA, compute Ξ_{Fit} for Eqs (4)–(9).

Accumulate: Transmute $W_{GA\text{-}IPA}$, time, iterations, function counts and Ξ_{Fit} for the IPA trials.

IPA process End

GA is known as a famous global search optimization method applied to solve the solve the constrained/unconstrained models efficiently. It is commonly implemented to regulate the precise population outcomes for solving the various stiff and complex models using the optimal training process. For the best solutions of the model, GA is implemented through the process of selection, reproduction, mutation and crossover procedures. Recently, GA is applied in many famous applications that can be seen in [28–32] and references cited therein.

IPA is a local search, rapid and quick optimization method, implemented to solve various reputed complex and non-stiff models efficiently. IPA is implemented in various models like phase-field approach to brittle and ductile fracture [33], multistage nonlinear nonconvex programs [34], SITR model for dynamics of novel coronavirus [35], viscoplastic fluid flows [36] and security constrained optimal power flow problems [37]. To control the Laziness of the global search method GA, the process of hybridization with the IPA is applied for solving the nonlinear smoke model. The detailed pseudocode based on the GNNs-GA-IPA is provided in Table 1.

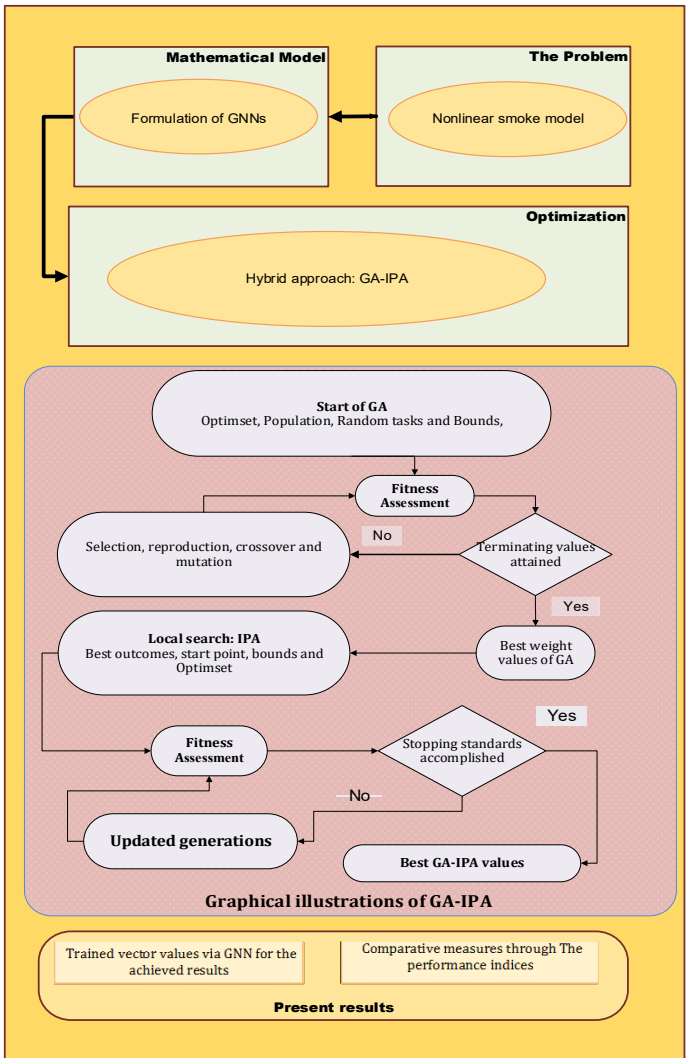

Figure 1. Designed framework of the GNNs-GA-IPA to solve the nonlinear smoke model.

3. Performance measures

The mathematical presentations using the statistical operators with "variance account for (VAF)", "Theil's inequality coefficient (TIC)", "mean absolute deviation (MAD)" and "semi interquartile (SI) range" together with the global operators G.VAF, G-TIC G-MAD are accessible to solve the nonlinear smoke model, written as:

$$\begin{cases} [\text{V.A.F}_P, \text{V.A.F}_S, \text{V.A.F}_{Q_T}, \text{V.A.F}_{Q_S}] = \begin{bmatrix} \left(1 - \frac{var(P_m - \hat{P}_m)}{var(P_m)}\right) \times 100, \\ \left(1 - \frac{var(S_m - \hat{S}_m)}{var(S_m)}\right) \times 100, \\ \left(1 - \frac{var((Q_T)_m - (\hat{Q}_T)_m)}{var(Q_T)_m}\right) \times 100, \\ \left(1 - \frac{var((Q_S)_m - (\hat{Q}_S)_m)}{var(Q_S)_m}\right) \times 100 \end{bmatrix}, \\ [\text{E-V.A.F}_P, \text{E-V.A.F}_S, \text{E-V.A.F}_{Q_T}, \text{E-V.A.F}_{Q_S}] = \begin{bmatrix} 100 - \text{V.A.F}_P, 100 - \text{V.A.F}_S, \\ 100 - \text{V.A.F}_{Q_T}, 100 - \text{V.A.F}_{Q_S} \end{bmatrix}. \end{cases} \tag{10}$$

$$\left[\mathrm{T.I.C}_P, \mathrm{T.I.C}_S, \mathrm{T.I.C}_{Q_T}, \mathrm{T.I.C}_{Q_S}\right] =$$

$$\left[\begin{array}{l} \frac{\sqrt{\frac{1}{n}\sum_{m=1}^{n}(P_m-\hat{P}_m)^2}}{\left(\sqrt{\frac{1}{n}\sum_{m=1}^{n}P_m^2}+\sqrt{\frac{1}{n}\sum_{m=1}^{n}\hat{P}_m^2}\right)}, \frac{\sqrt{\frac{1}{n}\sum_{m=1}^{n}(S_m-\hat{S}_m)^2}}{\left(\sqrt{\frac{1}{n}\sum_{m=1}^{n}S_m^2}+\sqrt{\frac{1}{n}\sum_{m=1}^{n}\hat{S}_m^2}\right)}, \\ \frac{\sqrt{\frac{1}{n}\sum_{m=1}^{n}((Q_T)_m-(\hat{Q}_T)_m)^2}}{\left(\sqrt{\frac{1}{n}\sum_{m=1}^{n}(Q_T)_m^2}+\sqrt{\frac{1}{n}\sum_{m=1}^{n}(\hat{Q}_T)_m^2}\right)}, \\ \frac{\sqrt{\frac{1}{n}\sum_{m=1}^{n}((Q_S)_m-(\hat{Q}_S)_m)^2}}{\left(\sqrt{\frac{1}{n}\sum_{m=1}^{n}(Q_S)_m^2}+\sqrt{\frac{1}{n}\sum_{m=1}^{n}(\hat{Q}_S)_m^2}\right)} \end{array}\right], \tag{11}$$

$$[\mathrm{M.A.D}_P, \mathrm{M.A.D}_S, \mathrm{M.A.D}_{Q_T}, \mathrm{M.A.D}_{Q_S}] =$$

$$\left[\begin{array}{l} \sum_{m=1}^{n}\left|P_m-\hat{P}_m\right|, \sum_{m=1}^{n}\left|S_m-\hat{S}_m\right|, \\ \sum_{m=1}^{n}\left|(Q_T)_m-\left(\hat{Q}_T\right)_m\right|, \sum_{m=1}^{n}\left|(Q_S)_m-\left(\hat{Q}_S\right)_m\right| \end{array}\right] \tag{12}$$

$$\begin{cases} \text{S.I Range} = -0.5\times(Q_1-Q_3), \\ Q_1 = 1^{st}\text{quartile} \qquad\qquad Q_3 = 3^{rd}\text{quartile}. \end{cases} \tag{13}$$

$\hat{P}$, $\hat{S}$, $\hat{Q}_T$ and $\hat{Q}_S$ are the approximate form of the solutions.

4. Results and simulations

The current investigations are associated to solve the nonlinear smoke model. The relative performance of the obtained solutions with the Runge-Kutta results is tested to show the exactness of the GNNs-GA-IPA. Moreover, the statistical operator's performances are used to validate the accuracy, reliability and precision of the proposed GNNs-GA-IPA. The updated form of the nonlinear smoke model given in the system (1) along with its ICs using the appropriate parameter values is shown as:

$$\begin{cases} P'(\Omega) = 20-(20P(\Omega)+0.003P(\Omega)S(\Omega)), P(0)=0.3, \\ S'(\Omega) = 0.003P(\Omega)S(\Omega)-20.3S(\Omega)+3Q_T(\Omega), S(0)=0.5, \\ Q_T'(\Omega) = 0.15S(\Omega)-23Q_T(\Omega), Q_T(0)=0.1, \\ Q_P'(\Omega) = 0.15S(\Omega)-20Q_P(\Omega), Q_P(0)=0.2, \end{cases} \tag{14}$$

A fitness function for the nonlinear smoke model (14) is written as:

$$\Xi_{Fit} =$$

$$\frac{1}{N}\sum_{m=1}^{N}\left(\begin{array}{l} \left[\hat{P}_m'+20\hat{P}_m-20+0.003\hat{P}_m\hat{S}_m\right]^2+\left[\hat{S}_m'+20.3\hat{S}_m-0.003\hat{P}_m\hat{S}_m-3(Q_T)_m\right]^2 \\ +\left[(Q_T')_m+23(Q_T)_m-0.15\hat{S}_m\right]^2+\left[(Q_P')_m+20(Q_P)_m-0.15\hat{S}_m\right]^2 \end{array}\right) \tag{15}$$

$$+\frac{1}{4}\left[\left(\hat{P}_0-0.3\right)^2+\left(\hat{S}_0-0.5\right)^2+((Q_T)_0-0.1)^2+((Q_P)_0-0.2)^2\right].$$

The performance of the scheme is observed based on the nonlinear smoke system using the GNNs-GA-IPA for 20 independent executions using 30 numbers of variables. The proposed form of the solution based on the nonlinear smoke model is provided in the arrangement of best weights using

the below equations for each group of the nonlinear smoke model and the graphical illustrations of these weights are plotted in Figure 2.

$$\begin{aligned}\hat{P}(\Omega) = {} & 7.2965(2\,tan^{-1}\,e^{(-5.343\Omega-18.462)} - 0.5\pi) - \\ & 2.7636(2\,tan^{-1}\,e^{1.2606\Omega+0.5134)} - 0.5\pi) \\ & +15.294(2\,tan^{-1}\,e^{(1.1551\Omega+2.0601)} - 0.5\pi) + \\ & 8.7324(2\,tan^{-1}\,e^{(19.759\Omega+2.9789)} - 0.5\pi) \\ & -7.1646(2\,tan^{-1}\,e^{(2.5198\Omega+5.9852)} - 0.5\pi) - \\ & 0.0053(2\,tan^{-1}\,e^{(-0.246\Omega-1.7692)} - 0.5\pi) \\ & -2.6104(2\,tan^{-1}\,e^{(0.2323\Omega+1.5497)} - 0.5\pi) - \\ & 1.4677(2\,tan^{-1}\,e^{(02.782\Omega+2.0890)} - 0.5\pi) \\ & +2.4715(2\,tan^{-1}\,e^{(-18516\Omega-3.253)} - 0.5\pi) - \\ & 2.9189(2\,tan^{-1}\,e^{(10.272\Omega-7.2465)} - 0.5\pi),\end{aligned} \tag{16}$$

$$\begin{aligned}\hat{S}(\Omega) = {} & 7.6303(2\,tan^{-1}\,e^{(-0.143\Omega+0.4605)} - 0.5\pi) + \\ & 9.6607(2\,tan^{-1}\,e^{(0.264\Omega+0.8726)} - 0.5\pi) \\ & -1.8710(2\,tan^{-1}\,e^{(0.3252\Omega-1.0967)} - 0.5\pi) + \\ & 0.0451(2\,tan^{-1}\,e^{(-1.961\Omega+8.4961)} - 0.5\pi) \\ & +5.4711(2\,tan^{-1}\,e^{(-9.8369\Omega-1.533)} - 0.5\pi) - \\ & 1.7275(2\,tan^{-1}\,e^{(-9.2138\Omega-2.037)} - 0.5\pi) \\ & +0.2908(2\,tan^{-1}\,e^{(-2.4236\Omega-0.378)} - 0.5\pi) - \\ & 1.9171(2\,tan^{-1}\,e^{(-9.2376\Omega-0.360)} - 0.5\pi) \\ & +2.7144(2\,tan^{-1}\,e^{(2.8428\Omega-7.8525)} - 0.5\pi) - \\ & 5.3000(2\,tan^{-1}\,e^{(-4.6148\Omega+4.164)} - 0.5\pi),\end{aligned} \tag{17}$$

$$\begin{aligned}\hat{Q}_T(\Omega) = {} & -0.563(2\,tan^{-1}\,e^{(-3.245\Omega+2.3616)} - 0.5\pi) - \\ & 0.022(2\,tan^{-1}\,e^{(-8.9859+1.2373)} - 0.5\pi) \\ & -0.5360(2\,tan^{-1}\,e^{(3.2982\Omega-2.4088)} - 0.5\pi) - \\ & 2.1382(2\,tan^{-1}\,e^{(-3.87\Omega-3.100)} - 0.5\pi) \\ & -4.7812(2\,tan^{-1}\,e^{(-4.1182\Omega-4.994)} - 0.5\pi) + \\ & 0.9505(2\,tan^{-1}\,e^{(-0.038\Omega-0.241)} - 0.5\pi) \\ & +17.841(2\,tan^{-1}\,e^{(-14.7536\Omega-4.557)} - 0.5\pi) - \\ & 3.4575(2\,tan^{-1}\,e^{(4.347\Omega+0.7343)} - 0.5\pi) \\ & +11.8361(2\,tan^{-1}\,e^{(4.5451\Omega+2.013)} - 0.5\pi) + \\ & 2.717(2\,tan^{-1}\,e^{(3.6697\Omega+7.33831)} - 0.5\pi),\end{aligned} \tag{18}$$

$$\begin{aligned}\hat{Q}_S(\Omega) = {} & 0.0762(2\,tan^{-1}\,e^{(2.9990\Omega+2.8605)} - 0.5\pi) + \\ & 2.8390(2\,tan^{-1}\,e^{(8.3177\Omega+0.6804)} - 0.5\pi) \\ & +7.6702(2\,tan^{-1}\,e^{(-0.0481\Omega+1.9373)} - 0.5\pi) - \\ & 0.4142(2\,tan^{-1}\,e^{(-0.309\Omega-0.401)} - 0.5\pi) \\ & -6.2827(2\,tan^{-1}\,e^{(1.2291\Omega+3.5918)} - 0.5\pi) + \\ & 0.5077(2\,tan^{-1}\,e^{(1.0574\Omega+1.0166)} - 0.5\pi) \\ & +2.2061(2\,tan^{-1}\,e^{(1.5133\Omega+10.7487)} - 0.5\pi) - \\ & 0.2776(2\,tan^{-1}\,e^{(1.7337\Omega+5.1928)} - 0.5\pi) \\ & -5.3623(2\,tan^{-1}\,e^{(8.4564\Omega+1.3100)} - 0.5\pi) + \\ & 0.0684(2\,tan^{-1}\,e^{(-4.1583\Omega-1.6646)} - 0.5\pi),\end{aligned} \tag{19}$$

A fitness function shown in the model (15) is optimized along with the hybridization of GA-IPA for the nonlinear smoke system. The proposed form of the outcomes is found using the above systems (16)–(19) for 30 variables between 0 to 1 input along with step size 0.1. The solutions of the nonlinear smoke model along with the best weight vector values are illustrated in Figures 2(a–d). The comparison of the mean and best outcomes with the reference Runge-Kutta solutions is provided in Figures 2(e–h) to solve the nonlinear smoke system. It is noticed that the mean and best results obtained by the GNNs-GA-IPA are overlapped with the reference results to solve each group of the nonlinear smoke model, which authenticate the exactness of the designed GNNs-GA-IPA. Figure 3 illustrates the values of the absolute error (AE) for each group of the nonlinear smoke model. It is observed that the values of the best AE for the group of potential smokers, smoker; temporary smoker and permanent smoker lie around 10-05-10-07, 10-05-10-06, 10-04-10-07 and 10-04-10-06, respectively. While, the mean AE values for these groups of the nonlinear smoke model found around 10-03-10-04, 10-03-10-05, 10-02-10-04 and 10-03-10-04, respectively. Figure 4 signifies the performance measures based on the operators EVAF, MAD and TIC to solve each group of the nonlinear smoke model. It is specified in the plots that the best values of the EVAF, MAD and TIC performances of each group of the nonlinear smoke model lie around 10-04-10-08, 10-03-10-05 and 10-08-10-09, respectively. The best performances of the EVAF, MAD and TIC for the $\hat{P}(\Omega)$ and $\hat{S}(\Omega)$ groups lie around 10-08-10-09, 10-05-10-06 and 10-09-10-10, respectively. The best performances of the EVAF, MAD and TIC for the $\hat{Q}_T(\Omega)$ group of the nonlinear smoke model found around 10-05-10-06, 10-04-10-06 and 10-08-10-10 and the best performances of the EVAF, MAD and TIC for the $\hat{Q}_P(\Omega)$ group of the nonlinear smoke model found around 10-07-10-08, 10-05-10-06 and 10-09-10-10. One can accomplish from the indications that the designed GNNs-GA-IPA is precise and accurate.

The graphic illustrations based on the statistical performances are provided in Figures 5–7 to find the convergence along with the boxplots and the histograms to solve the nonlinear smoke model. Figure 5 shows the performance of TIC for twenty runs to solve each group of the nonlinear smoke model. It is observed that most of the executions for the $\hat{P}$, $\widehat{S}$, $\hat{Q}_T$ and $\hat{Q}_S$ groups lie around 10-07-10-10. The MAD performances are illustrated in Figure 6 that depicts most of the executions for the $\hat{P}$, $\widehat{S}$, $\hat{Q}_T$ and $\hat{Q}_S$ groups lie around 10-03-10-05. The EVAF performances are illustrated in Figure 7 that depicts most of the executions for the $\hat{P}$, $\widehat{S}$, $\widehat{Q}_T$ and $\hat{Q}_S$ groups lie around 10-04-10-08. The best trial performances using the GNNs-GA-IPA are calculated suitable for the TIC, EVAF and MAD operators.

The routines for different statistical operators, Maximum (Max), Median, Minimum (Min), standard deviation (STD) and SIR are provided in Tables 2–5 to validate the accurateness and precision to solve the $\hat{P}$, $\widehat{S}$, $\widehat{Q}_T$ and $\hat{Q}_S$ groups of the nonlinear smoke system. The Max operators indicate the worst solutions, whereas the Min operators show the best results using 20 independent runs. For the group $P(\Omega)$, $S(\Omega)$, $Q_T(\Omega)$ and $Q_S(\Omega)$ of the nonlinear smoke model, the 'Max' and 'Min' standards lie around 10-03-10-04 and 10-06-10-08, while the Median, SIR, STD and Mean standards lie around 10-04-10-05. These small values designate the worth and values of the GNNs-GA-IPA to solve each group of the nonlinear smoke model. One can observe through these calculate measures, that the designed GNNs-GA-IPA is precise, accurate and stable.

The global performances of the G.EVAF, G.MAD and G.TIC operators for twenty runs to solve the designed GNNs-GA-IPA are provided in Table 6 to solve each group of the nonlinear smoke model. These Min global G.MAD, G.TIC and G.EVAF performances found around 10-04-10-05, 10-08-10-09

and 10-05-10-07, whereas the SIR global values lie in the ranges of 10-04-10-05, 10-08-10-09 and 10-04-10-07 for all groups of the nonlinear smoke model. These close optimal global measures values demonstrate the correctness, accurateness and precision of the proposed GNNs-GA-IPA.

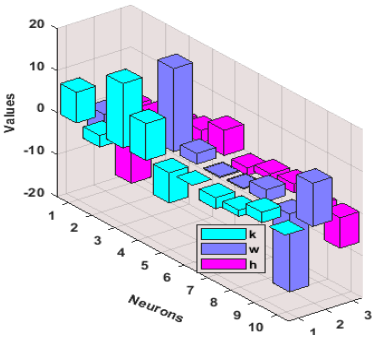

(a) $P(\Omega)$: Best weights.

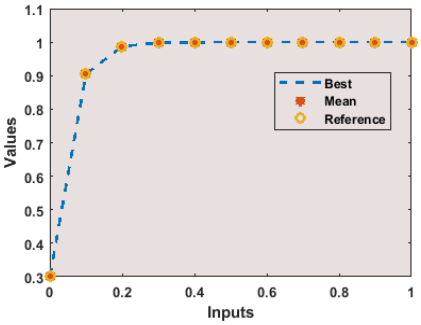

(e) Results for group $P(\Omega)$.

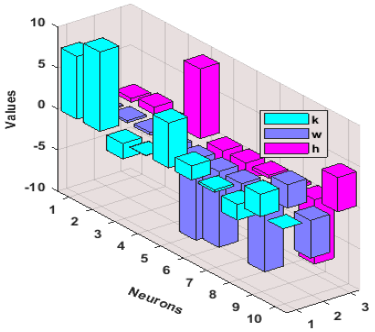

(b) $S(\Omega)$: Best weights.

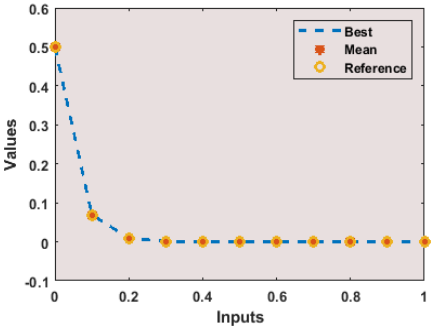

(f) Results for group $S(\Omega)$.

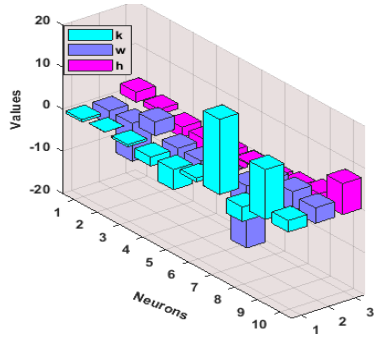

(c) $Q_T(\Omega)$: Best weights.

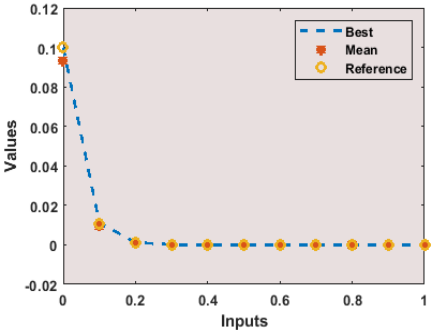

(g) Results for group $Q_T(\Omega)$.

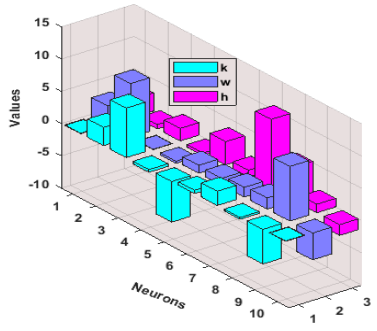

(d) $Q_S(\Omega)$: Best weights.

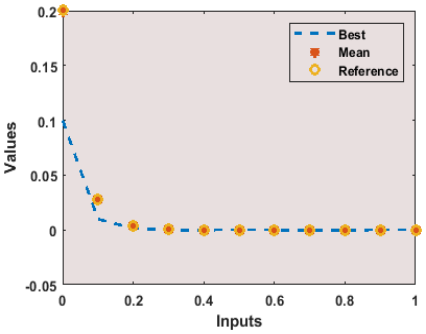

(h) Results for group $Q_S(\Omega)$.

Figure 2. Best weight vectors along with the result comparisons of the mean and best results with reference results to solve the nonlinear smoke model.

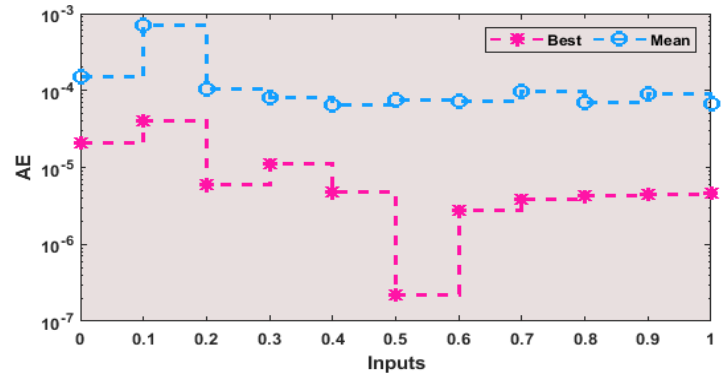

(a) AE for the group P(Ω).

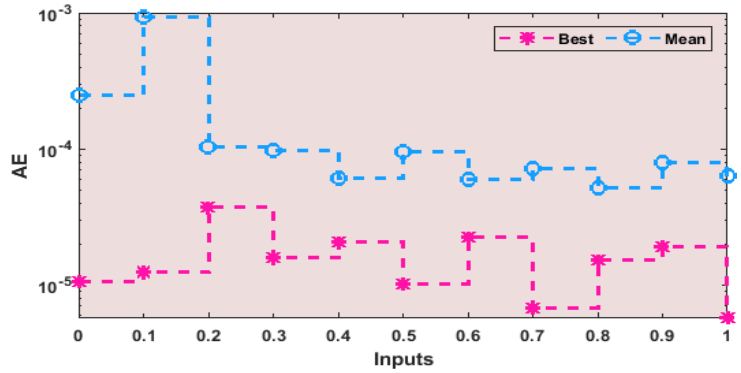

(b) AE for the group S(Ω).

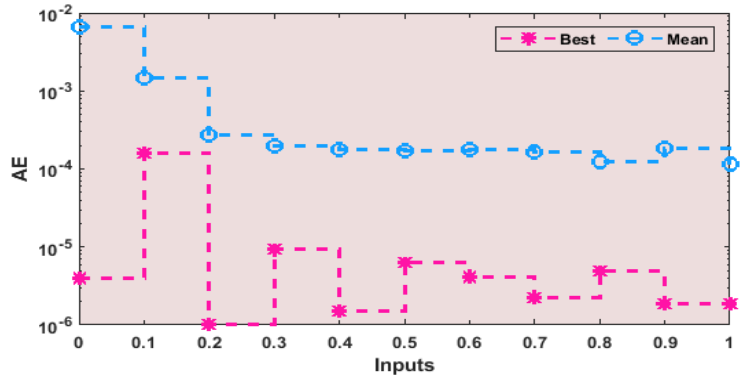

(c) AE for the group QT(Ω).

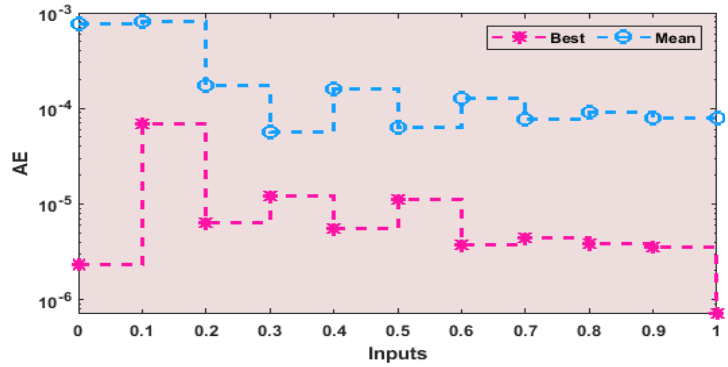

(d) AE for the group QS(Ω).

Figure 3. AE values for each group of the nonlinear smoke system.

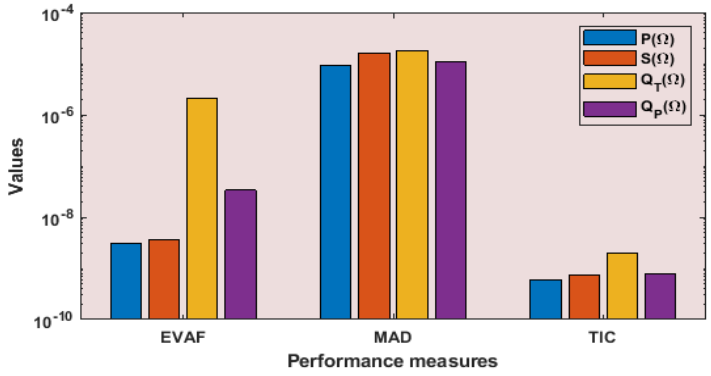

Figure 4. Performances based on EVAF, MAD and TIC values to solve each group of the nonlinear smoke model.

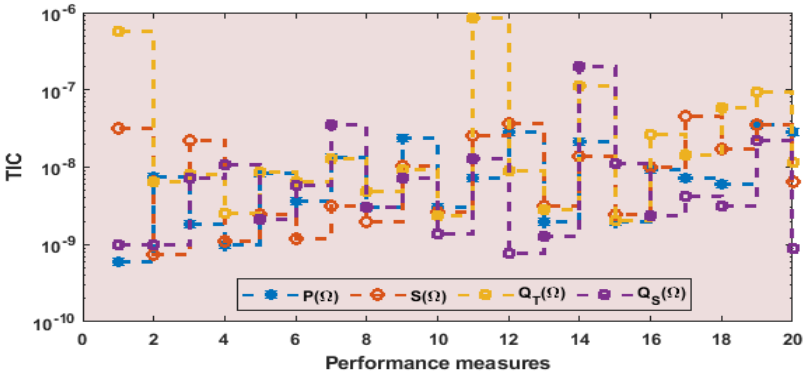

Performance of TIC for each group of the nonlinear smoke model.

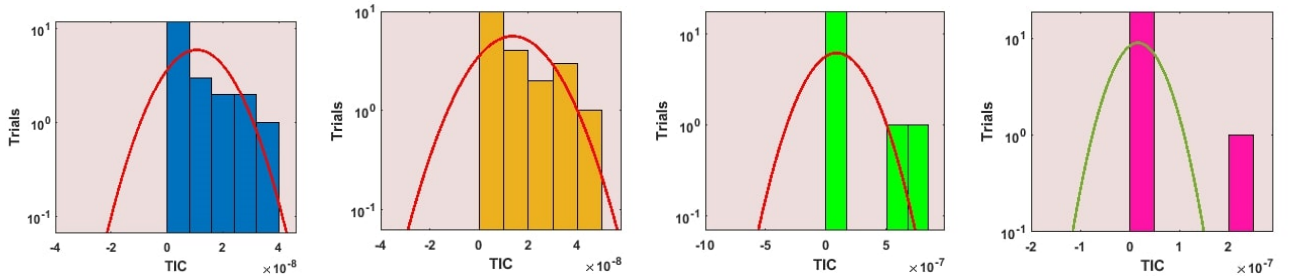

Histogram: $P(\Omega)$ group. Histogram: $Sp(\Omega)$ group. Histogram: $QT(\Omega)$ group. Histogram: $QS(\Omega)$ group.

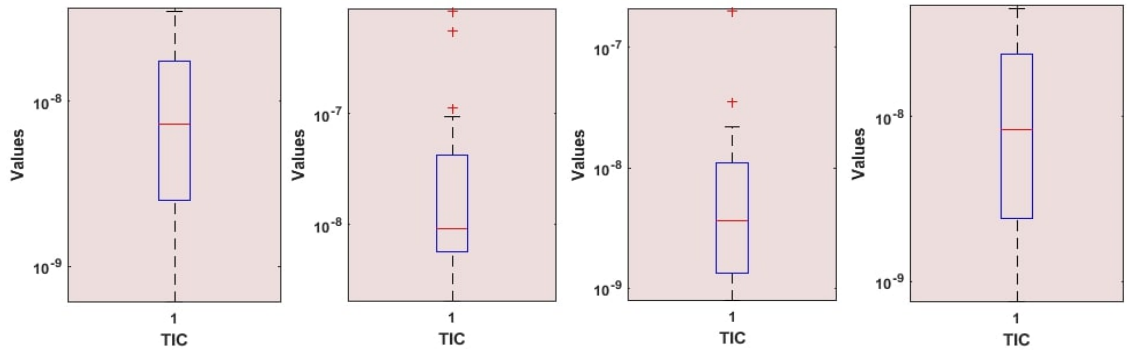

Boxplots: $P(\Omega)$ group. Boxplots: $Sp(\Omega)$ group. Boxplots: $Qp(\Omega)$ group. Boxplots: $QS(\Omega)$ group.

Figure 5. Convergence of the TIC values along with the Boxplots and histograms to solve each group of the nonlinear smoke model.

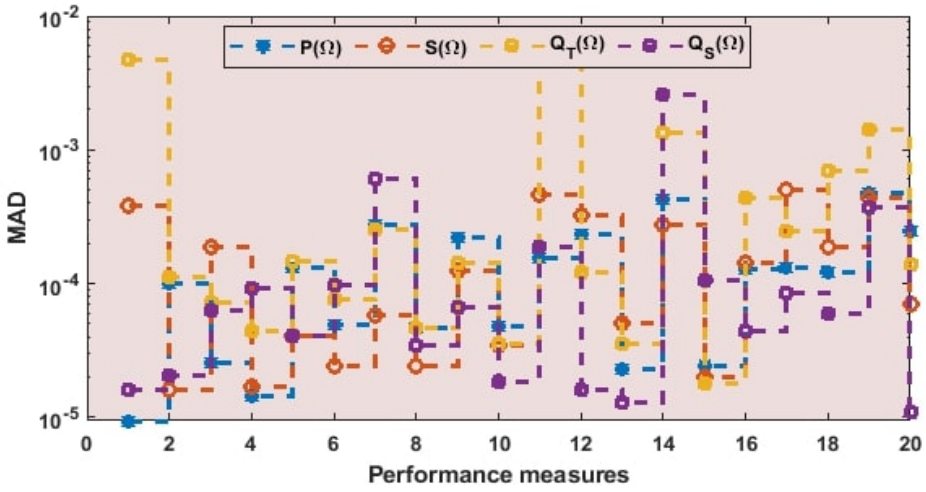

Performance of MAD for each group of the nonlinear smoke model.

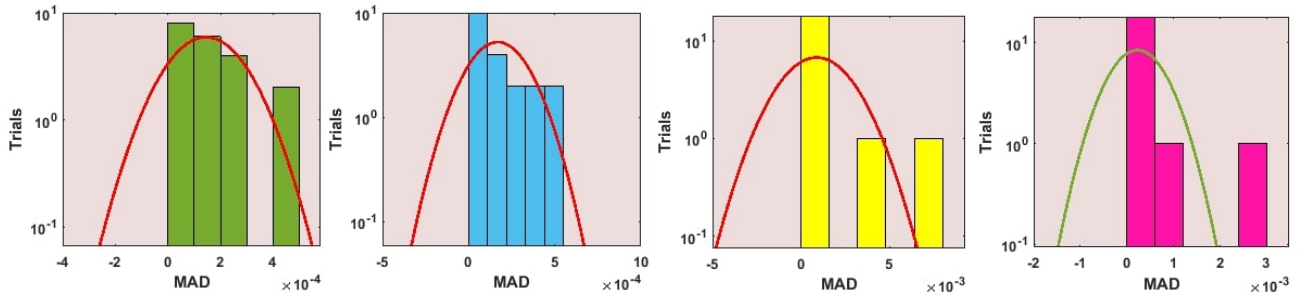

Histogram: P(Ω) group. Histogram: S p(Ω) group. Histogram: QT(Ω) group. Histogram: QS(Ω) group.

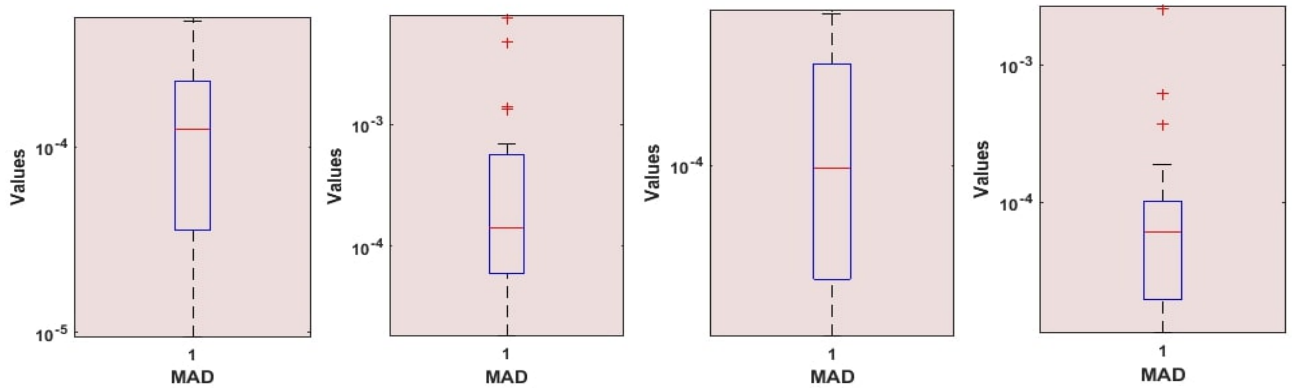

Boxplots: P(Ω) group. Boxplots: Sp(Ω) group. Boxplots: Qp(Ω) group. Boxplots: QS(Ω) group.

Figure 6. Convergence of the MAD values along with the Boxplots and histograms to solve each group of the nonlinear smoke model.

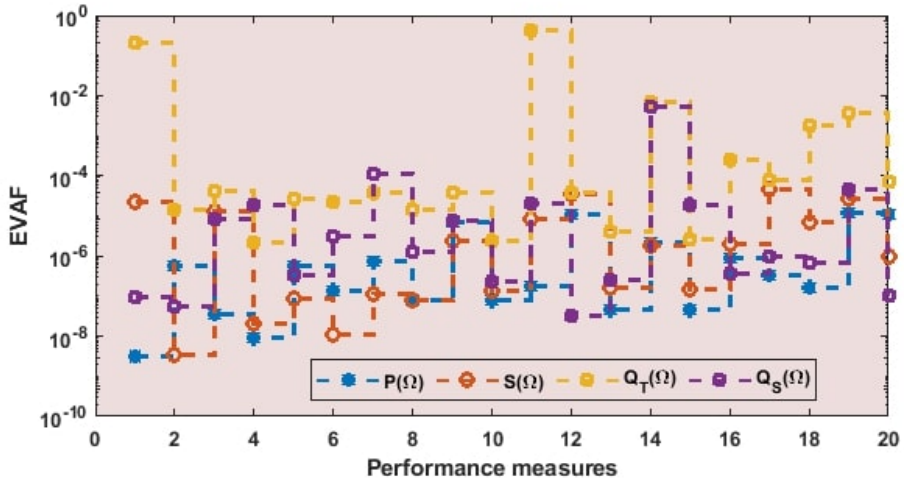

Performance of EVAF for each group of the nonlinear smoke model.

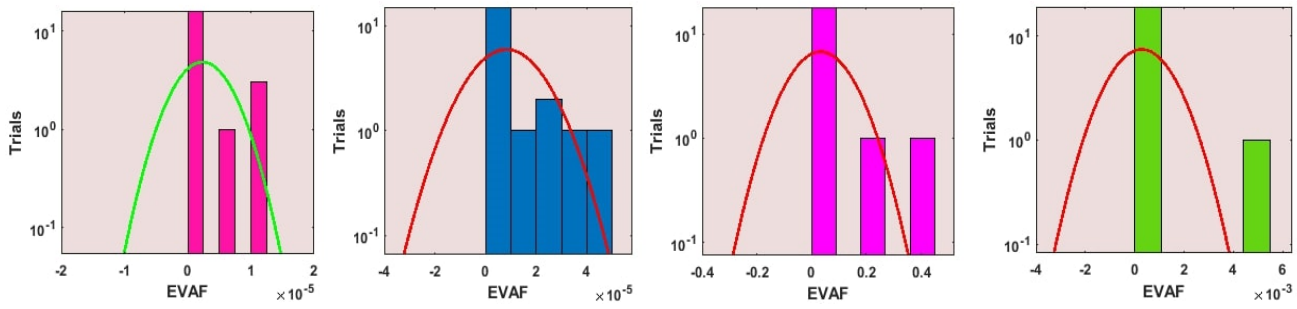

Histogram: P(Ω) group. Histogram: S p(Ω) group. Histogram: QT(Ω) group. Histogram: QS(Ω) group.

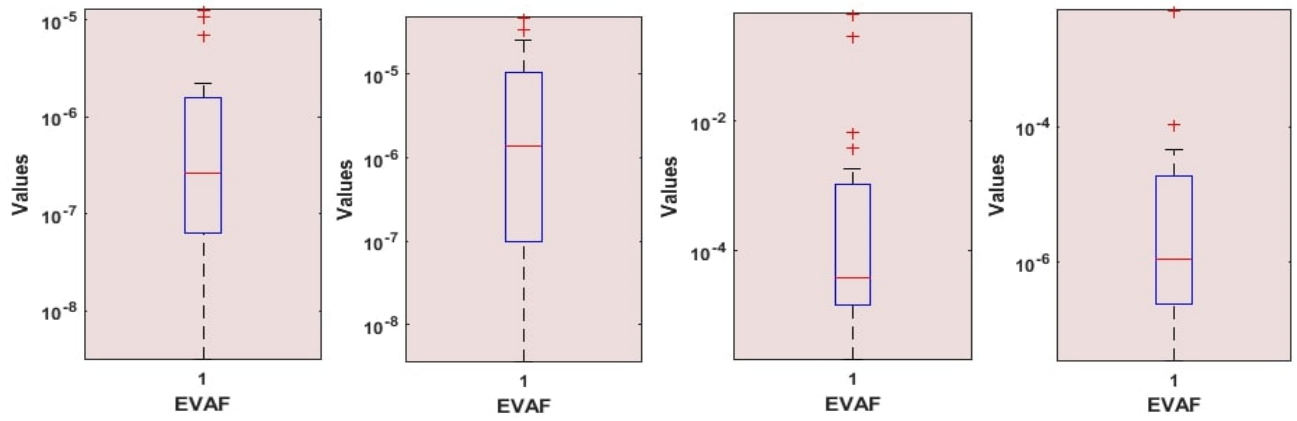

Boxplots: P(Ω) group. Boxplots: Sp(Ω) group. Boxplots: Qp(Ω) group. Boxplots: QS(Ω) group.

Figure 7. Convergence of the EVAF values along with the Boxplots and histograms to solve each group of the nonlinear smoke model.

Table 2. Statistical measures for the nonlinear smoke model of group $P(\Omega)$.

Ω	P(Ω)					
	Max	Min	Median	STD	SIR	Mean
0	1.9698E-03	1.5128E-07	1.3179E-05	4.3988E-04	2.8322E-05	1.5255E-04
0.1	2.2927E-03	4.0452E-05	3.7091E-04	7.5870E-04	3.5757E-04	7.1580E-04
0.2	2.8517E-04	2.5715E-06	8.0076E-05	1.0291E-04	8.7298E-05	1.0480E-04
0.3	3.7540E-04	5.0221E-06	4.6631E-05	9.6615E-05	5.7759E-05	8.0291E-05
0.4	3.1095E-04	7.2215E-07	2.5169E-05	7.9915E-05	4.8322E-05	6.4497E-05
0.5	3.7039E-04	1.0187E-07	4.0958E-05	9.9187E-05	4.0049E-05	7.4737E-05
0.6	3.4788E-04	2.7497E-06	3.6783E-05	8.6814E-05	5.3154E-05	7.3405E-05
0.7	7.2524E-04	3.8591E-06	2.6741E-05	1.6887E-04	5.3778E-05	9.7130E-05
0.8	3.1439E-04	2.3193E-06	3.0315E-05	8.9765E-05	3.8282E-05	6.8701E-05
0.9	8.2385E-04	3.6579E-06	3.6581E-05	1.8035E-04	2.2583E-05	8.9806E-05
1	3.9210E-04	8.9543E-07	1.4825E-05	1.1497E-04	3.4368E-05	6.7763E-05

Table 3. Statistical measures for the nonlinear smoke model of group $S(\Omega)$.

Ω	$S(\Omega)$					
	Max	Min	Median	STD	SIR	Mean
0	2.2510E-03	8.8331E-07	1.5049E-05	4.3988E-04	6.5800E-05	2.4625E-04
0.1	3.5749E-03	1.2621E-05	4.2711E-04	7.5870E-04	5.9138E-04	9.2693E-04
0.2	5.8967E-04	6.8508E-06	5.0534E-05	1.0291E-04	3.8159E-05	1.0389E-04
0.3	3.9412E-04	4.5897E-07	5.5860E-05	9.6615E-05	4.8082E-05	9.7091E-05
0.4	1.8148E-04	1.4261E-06	3.2627E-05	7.9915E-05	4.6977E-05	6.1366E-05
0.5	3.8406E-04	3.0499E-06	5.0425E-05	9.9187E-05	4.5676E-05	9.6411E-05
0.6	3.3693E-04	1.0786E-06	3.2525E-05	8.6814E-05	2.6474E-05	5.9807E-05
0.7	3.8976E-04	5.9658E-08	3.4605E-05	1.6887E-04	3.0731E-05	7.1943E-05
0.8	4.6451E-04	1.8083E-07	2.9100E-05	8.9765E-05	1.9639E-05	5.1752E-05
0.9	3.7056E-04	5.8454E-07	3.1691E-05	1.8035E-04	4.5808E-05	7.8891E-05
1	3.4425E-04	3.5833E-08	3.7245E-05	1.1497E-04	2.5924E-05	6.3636E-05

Table 4. Statistical measures for the nonlinear smoke model of group $Q_T(\Omega)$.

Ω	$Q_T(\Omega)$					
	Max	Min	Median	STD	SIR	Mean
0	6.7379E-02	2.0435E-06	7.4367E-05	4.3988E-04	1.2547E-03	6.6320E-03
0.1	8.8212E-03	1.5933E-04	6.6896E-04	7.5870E-04	6.4736E-04	1.4858E-03
0.2	1.2208E-03	1.0177E-06	1.6681E-04	1.0291E-04	1.3929E-04	2.7755E-04
0.3	1.2039E-03	6.2163E-06	3.5966E-05	9.6615E-05	7.5659E-05	2.0075E-04
0.4	5.2048E-04	1.5004E-06	9.3199E-05	7.9915E-05	1.4812E-04	1.7703E-04
0.5	7.9163E-04	4.1214E-06	7.5760E-05	9.9187E-05	9.4190E-05	1.7072E-04
0.6	7.5113E-04	3.4495E-06	5.6836E-05	8.6814E-05	1.5865E-04	1.8051E-04
0.7	6.9564E-04	2.1601E-06	8.7570E-05	1.6887E-04	1.2891E-04	1.6565E-04
0.8	8.5659E-04	2.3356E-06	5.6424E-05	8.9765E-05	6.5358E-05	1.2238E-04
0.9	8.5832E-04	1.8869E-06	8.6636E-05	1.8035E-04	1.2103E-04	1.8340E-04
1	5.9922E-04	9.8962E-07	3.9188E-05	1.1497E-04	4.8965E-05	1.1550E-04

Table 5. Statistical measures for the nonlinear smoke model of group $Q_S(\Omega)$.

Ω	$Q_S(\Omega)$					
	Max	Min	Median	STD	SIR	Mean
0	1.4249E-02	4.6038E-07	1.0193E-05	3.1752E-03	5.3007E-05	7.6325E-04
0.1	7.1456E-03	9.4140E-06	2.0718E-04	1.6018E-03	3.9882E-04	8.1152E-04
0.2	1.4449E-03	2.1615E-07	2.8536E-05	3.6835E-04	3.0447E-05	1.7480E-04
0.3	3.7091E-04	3.2754E-07	2.1791E-05	8.7324E-05	2.6186E-05	5.6609E-05
0.4	1.5545E-03	1.8846E-07	2.2389E-05	3.7612E-04	6.1143E-05	1.5810E-04
0.5	3.7972E-04	3.6651E-06	1.7656E-05	9.8654E-05	3.1268E-05	6.2521E-05
0.6	1.2224E-03	2.4032E-07	2.1050E-05	2.9478E-04	3.3053E-05	1.2732E-04
0.7	7.4101E-04	1.7539E-07	2.4276E-05	1.6625E-04	2.5398E-05	7.7130E-05
0.8	1.0726E-03	2.5213E-06	1.4100E-05	2.3771E-04	3.0541E-05	9.1329E-05
0.9	7.4407E-04	2.5770E-06	3.5282E-05	1.6258E-04	2.8865E-05	7.9482E-05
1	9.7616E-04	7.0693E-07	8.9328E-06	2.1858E-04	1.0034E-05	8.0351E-05

Table 6. Global measures based on the MAD, TIC and EVAF values to solve each group of the nonlinear smoke model.

Class	(G.MAD)		(G.TIC)		(G.EVAF)	
	Min	SIR	Min	SIR	Min	SIR
$P(\Omega)$	1.2499E-04	9.6058E-05	7.2597E-09	7.4459E-09	2.6155E-07	7.5331E-07
$S(\Omega)$	9.7570E-05	1.3353E-04	8.3068E-08	1.0766E-08	1.3879E-06	5.2293E-06
$Q_T(\Omega)$	1.4111E-04	2.5334E-04	9.1566E-09	1.8187E-08	3.9553E-05	5.1487E-04
$Q_S(\Omega)$	6.0979E-05	4.1189E-05	3.6367E-09	4.8515E-09	1.1015E-06	9.3296E-06

5. Reference style, citation, and cross-reference

The current investigations are related to solve the nonlinear smoke model by exploiting the Gudermannian neural networks using the global and local search methodologies, i.e., GNNs-GA-IPA. The smoke model is a system of nonlinear equations contain four groups temporary smokers, potential smokers, permanent smokers and smokers. For the numerical outcomes, a fitness function is established using all groups of the nonlinear smoke model and its corresponding ICs. The optimization of the fitness function using the hybrid computing framework of GNNs-GA-IPA for solving each group of the nonlinear smoke model. The Gudermannian function is designed as a merit function along with 30 numbers of variables. The overlapping of the proposed mean and best outcomes is performed with the Runge-Kutta reference results for each group of the nonlinear smoke model. These matching and reliable results to solve the nonlinear smoke model indicate the exactness of the designed GNNs-GA-IPA. In order to show the precision and accuracy of the proposed GNNs-GA-IPA, the statistical performances based on the TIC, MAD and EVAF operators have been accessible for twenty trials using 10 numbers of neurons. To check the performance analysis, most of the runs based on the statistical TIC, MAD and EVAF performances show a higher level of accuracy to solve each group of the nonlinear smoke model. The valuations using the statistical gages of Max, Min, Mean, STD, Med and SIR further validate the value of the proposed GNNs-GA-IPA. Furthermore, global presentations through SIR and Min have been applied for the nonlinear smoke model.

In future, the designed GNNs-GA-IPA is accomplished to solve the biological nonlinear

systems [38], singular higher order model [39], fluid dynamics nonlinear models [40] and fractional differential model [41].

Acknowledgments

The authors extend their appreciation to the Deanship of Scientific Research at Imam Mohammad Ibn Saud Islamic University for funding this work through Research Group no. RG-21-09-12.

Conflict of interest

All authors of the manuscript declare that there have no potential conflicts of interest.

References

1. B. Hipple, H. Lando, J. Klein, J. Winickoff, Global teens and tobacco: a review of the globalization of the tobacco epidemic, *Curr. Probl. Pediatr. Adolesc. Health Care*, **41** (2011), 216–230. doi: 10.1016/j.cppeds.2011.02.010.
2. *World Health Organization*, *WHO Report on the Global Tobacco Epidemic, 2009: Implementing Smoke-free Environments: Executive Summary*, 2009. Available from: http://apps.who.int/iris/bitstream/handle/10665/70429/WHO_NMH_TFI_09.1_eng.pdf;sequene=1.
3. C. Castillo-Garsow, G. Jordán-Salivia, A. Rodriguez-Herrera, Mathematical models for the dynamics of tobacco use, recovery and relapse, *Garsow*, (1997). Available from: https://hdl.handle.net/1813/32095.
4. O. Sharomi, A. B. Gumel, Curtailing smoking dynamics: a mathematical modeling approach, *Appl. Math. Comput.*, **195** (2008), 475–499. doi: 10.1016/j.amc.2007.05.012.
5. Z. Sabir, M. Umar, M. A. Z. Raja, D. Baleanu, Applications of Gudermannian neural network for solving the SITR fractal system, *Fractals*, (2021). doi: 10.1142/S0218348X21502509.
6. Z. Sabir, M. A. Z. Raja, D. Baleanu, R. Sadat, M. R. Ali, Investigations of nonlinear induction motor model using the Gudermannian neural networks, *Therm. Sci.*, (2021). doi: 10.2298/TSCI210508261S.
7. K. Nisar, Z, Sabir, M. A. Z. Raja, A. A. A. Ibrahim, D. B. Rawat, Evolutionary integrated heuristic with Gudermannian neural networks for second kind of Lane-Emden nonlinear singular models, *Appl. Sci.*, **11** (2021), 4725. doi: 10.3390/app11114725.
8. Z. Sabir, M. A. Z. Raja, A. Arbi, G. C. Altamirano, J. Cao, Neuro-swarms intelligent computing using Gudermannian kernel for solving a class of second order Lane-Emden singular nonlinear model, *AIMS Math.*, **6** (2021), 2468–2485. doi: 10.3934/math.2021150.
9. M. Higazy, A. M. S. Mahdy, N. H. Sweilam, Approximate solutions for solving nonlinear fractional order smoking model, *Alexandria Eng. J.*, **59** (2020), 739–752. doi: 10.1016/j.aej.2020.01.049.
10. A. M. S. Mahdy, Numerical studies for solving fractional integro-differential equations, *J. Ocean Eng. Sci.*, **3** (2018), 127–132. doi: 10.1016/j.joes.2018.05.004.
11. A. M. S. Mahdy, M. Higazy, K. A. Gepreel, A. A. A. El-dahdouh, Optimal control and bifurcation diagram for a model nonlinear fractional SIRC, *Alexandria Eng. J.*, **59** (2020), 3481–3501. doi: 10.1016/j.aej.2020.05.028.

12. J. Zhang, C. Chen, X. Yang, Y. Chu, Z. Xia, Efficient, non-iterative, and second-order accurate numerical algorithms for the anisotropic Allen-Cahn equation with precise nonlocal mass conservation, *J. Comput. Appl. Math.*, **363** (2020), 444–463. doi: 10.1016/j.cam.2019.05.003.
13. A. M. S. Mahdy, K. Lotfy, W. Hassan, A. A. El-Bary, Analytical solution of magneto-photothermal theory during variable thermal conductivity of a semiconductor material due to pulse heat flux and volumetric heat source, *Waves Random Complex Media*, (2020), 1–18. doi: 10.1080/17455030.2020.1717673.
14. K. Lotfy, Effect of variable thermal conductivity during the photothermal diffusion process of semiconductor medium, *Silicon*, **11** (2019), 1863–1873. doi: 10.1007/s12633-018-0005-z.
15. I. Ahmad, H. Ilyas, M. A. Z. Raja, Z. Khan, M. Shoaib, Stochastic numerical computing with Levenberg-Marquardt backpropagation for performance analysis of heat sink of functionally graded material of the porous fin, *Surf. Interfaces*, **26** (2021), 101403. doi: 10.1016/j.surfin.2021.101403.
16. H. Ilyas, A. Iftikhar, M. A. Z. Raja, M. B. Tahir, M Shoaib, Intelligent computing for the dynamics of fluidic system of electrically conducting Ag/Cu nanoparticles with mixed convection for hydrogen possessions, *Int. J. Hydrogen Energy*, **46** (2021), 4947–4980. doi: 10.1016/j.ijhydene.2020.11.097.
17. T. N. Cheema, M. A. Z. Raja, A. Iftikhar, S. Naz, M. Shoaib, Intelligent computing with Levenberg-Marquardt artificial neural networks for nonlinear system of COVID-19 epidemic model for future generation disease control, *Eur. Phys. J. Plus*, **135** (2020), 1–35. doi: 10.1140/epjp/s13360-020-00910-x.
18. Z. Sabir, M. A.Z. Raja, M. Umar, M. Shoaib, Design of neuro-swarming-based heuristics to solve the third-order nonlinear multi-singular Emden-Fowler equation, *Eur. Phys. J. Plus*, **135** (2020), 1–17. doi: 10.1140/epjp/s13360-020-00424-6.
19. Z. Sabir, M. A. Z. Raja, M. Umar, M. Shoaib, Neuro-swarm intelligent computing to solve the second-order singular functional differential model, *Eur. Phys. J. Plus*, **135** (2020), 474. doi: 10.1140/epjp/s13360-020-00440-6.
20. M. Umar, Z, Sabir, M. A. Z. Raja, Y. G. Sánchez, A stochastic numerical computing heuristic of SIR nonlinear model based on dengue fever, *Results Phys.*, **19** (2020), 103585. doi: 10.1016/j.rinp.2020.103585.
21. A. K. Kiani, W. U. Khan, M. A. Z. Raja, Y. He, Z. Sabir, M. Shoaib, Intelligent backpropagation networks with bayesian regularization for mathematical models of environmental economic systems, *Sustainability*, **13** (2021), 9537. doi: 10.3390/su13179537.
22. M. Umar, Z. Sabir, M. A. Z. Raja, Intelligent computing for numerical treatment of nonlinear prey-predator models, *Appl. Soft Comput.*, **80** (2019), 506–524. doi: 10.1016/j.asoc.2019.04.022.
23. Z. Sabir, M. A. Manzar, M. A. Z. Raja, M. Sheraz, A. M. Wazwaz, Neuro-heuristics for nonlinear singular Thomas-Fermi systems, *Appl. Soft Comput.*, **65** (2018), 152–169. doi: 10.1016/j.asoc.2018.01.009.
24. M. Umar, M. A. Z. Raja, Z. Sabir, A. S. Alwabli, M. Shoaib, A stochastic computational intelligent solver for numerical treatment of mosquito dispersal model in a heterogeneous environment, *Eur. Phys. J. Plus*, **135** (2020), 1–23. doi: 10.1140/epjp/s13360-020-00557-8.
25. M. A. Z. Raja, U, Muhammad, S, Zulqurnain, K. J. Ali, B. Dumitru, A new stochastic computing paradigm for the dynamics of nonlinear singular heat conduction model of the human head, *Eur. Physical J. Plus*, **133** (2018), 364. doi: 10.1140/epjp/s13360-020-00557-8.

26. Z. Sabir, M. A. Z. Raja, M. Shoaib, J. F. G. Aguilar, FMNEICS: fractional Meyer neuro-evolution-based intelligent computing solver for doubly singular multi-fractional order Lane-Emden system, *Comput. Appl. Math.*, **39** (2020), 1–18. doi: 10.1007/s40314-020-01350-0.
27. M. Umar, Z. Sabir, M. Asif, Z. Raja, YG Sánchez, A stochastic intelligent computing with neuro-evolution heuristics for nonlinear SITR system of novel COVID-19 dynamics, *Symmetry*, **12** (2020), 1628. doi: 10.3390/sym12101628.
28. W. Han, B. Hua, X. Ruan, Genetic algorithm-driven discovery of unexpected thermal conductivity enhancement by disorder, *Nano Energy*, **71** (2020), 104619. doi: 10.1016/j.nanoen.2020.104619.
29. S. L. Podvalny, M. I. Chizhov, P. Y. Gusev, K. Y. Gusev, The crossover operator of a genetic algorithm as applied to the task of a production planning, *Procedia Comput. Sci.*, **150** (2019), 603–608. doi: 10.1016/j.procs.2019.02.100.
30. M. M. Gani, M. S. Islam, M. A. Ullah, Optimal PID tuning for controlling the temperature of electric furnace by genetic algorithm, *SN Appl. Sci.*, **1** (2019), 1–8. doi: 10.1007/s42452-019-0929-y.
31. S. Parinam, M. Kumar, N. Kumari, V. Karar, A. L. Sharma, An improved optical parameter optimisation approach using Taguchi and genetic algorithm for high transmission optical filter design, *Optik*, **182** (2019), 382–392. doi: 10.1016/j.ijleo.2018.12.189.
32. M. Hajipour, K. Etminani, Z. Rahmatinejad, M. Soltani, K. Etemad, S. Eslami, et al., A predictive model for mortality of patients with thalassemia using logistic regression model and genetic algorithm, *Int. J. Health Stud.*, **4** (2018), 21–26. doi: 10.22100/ijhs.v4i3.523.
33. J. Wambacq, J. Ulloa, G. Lombaert, S. Franois, Interior-point methods for the phase-field approach to brittle and ductile fracture, *Comput. Methods Appl. Mech. Eng.*, **375** (2021), 113612. doi: 10.1016/j.cma.2020.113612.
34. A. Zanelli, A. Domahidi, J. Jerez, M. Morari, FORCES NLP: an efficient implementation of interior-point methods for multistage nonlinear nonconvex programs, *Int. J. Control*, **93** (2020), 13–29. doi: 10.1080/00207179.2017.1316017.
35. M. Umar, Z. Sabir, M. A. Z. Raja, F. Amin, Y. G. Sanchez, Integrated neuro-swarm heuristic with interior-point for nonlinear SITR model for dynamics of novel COVID-19, *Alexandria Eng. J.*, **60** (2021), 2811–2824. doi: 10.1016/j.aej.2021.01.043.
36. J. Bleyer, Advances in the simulation of viscoplastic fluid flows using interior-point methods, *Comput. Methods Appl. Mech. Eng.*, **330** (2018), 368–394. doi: 10.1016/j.cma.2017.11.006.
37. J. Kardoš, D. Kourounis, O. Schenk, Two-level parallel augmented schur complement interior-point algorithms for the solution of security constrained optimal power flow problems, *IEEE Trans. Power Syst.*, **35** (2019), 1340–1350. doi: 10.1109/TPWRS.2019.2942964.
38. M. Umar, Z. Sabir, M. A. Z. Raja, J. F. Gómez Aguilar, F. Amin, M. Shoaib, Neuro-swarm intelligent computing paradigm for nonlinear HIV infection model with CD4+ T-cells, *Math. Comput. Simul.*, (2021). doi: 10.1016/j.matcom.2021.04.008.
39. Z. Sabir, M. A. Z. Raja, C. M. Khalique, C. Unlu, Neuro-evolution computing for nonlinear multi-singular system of third order Emden-Fowler equation, *Math. Comput. Simul.*, **185** (2021), 799–812. doi: 10.1016/j.matcom.2021.02.004.
40. M. Shoaib, M. A. Z. Raja, M. A. R. Khan, I. Farhat, S. E. Awan, Neuro-computing networks for entropy generation under the influence of MHD and thermal radiation, *Surf. Interfaces*, (2021), 101243. doi: 10.1016/j.surfin.2021.101243.

41. Z. Sabir, M. A. Z. Raja, J. L. G. Guirao, M. Shoaib, A novel design of fractional Meyer wavelet neural networks with application to the nonlinear singular fractional Lane-Emden systems, *Alexandria Eng. J.*, **60** (2021), 2641–2659. doi: 10.1016/j.aej.2021.01.004.

AIMS Press